OPEN ACCESS
IOP Publishing
Superconductor Science and Technology
Supercond. Sci. Technol. **31** (2018) 075001 (7pp)
https://doi.org/10.1088/1361-6668/aac290

Electrically tunable crossed Andreev reflection in a ferromagnet–superconductor–ferromagnet junction on a topological insulator

Kunhua Zhang[1,2] **and Qiang Cheng**[3]

[1] ICQD, Hefei National Laboratory for Physical Sciences at Microscale, University of Science and Technology of China, Hefei, Anhui 230026, People's Republic of China
[2] Theoretical Condensed Matter Physics and Computational Materials Physics Laboratory, School of Physics, University of Chinese Academy of Sciences, Beijing 100049, People's Republic of China
[3] School of Science, Qingdao Technological University, Qingdao, Shandong 266520, People's Republic of China

E-mail: zhangkh1@ustc.edu.cn

Received 25 January 2018, revised 27 April 2018
Accepted for publication 4 May 2018
Published 23 May 2018

Abstract

We investigate the crossed Andreev reflection in a ferromagnet–superconductor–ferromagnet junction on the surface of a topological insulator, where the magnetizations in the left and right leads are perpendicular to the surface. We find that the nonlocal transport process can be pure crossed Andreev reflection or pure elastic cotunneling, and the switch between the two processes can be controlled electrically. Pure crossed Andreev reflection appears for all bias voltages in the superconducting energy gap, which is independent of the configuration of the magnetizations in the two leads. The spin of the crossed Andreev reflected hole could be parallel to the spin of the incident electron, which is brought by the spin-triplet pairing correlation. The average transmission probability of crossed Andreev reflection can be larger than 90%, so a high efficiency nonlocal splitting of Cooper pairs can be generated, and turned on and off electrically.

Keywords: crossed Andreev reflection, splitting of Cooper pairs, spin-triplet pairing correlation, topological surface states

(Some figures may appear in colour only in the online journal)

1. Introduction

The entangled states of electrons have received much attention in solid state system for practical application in quantum information [1]. Superconductors have been considered as natural sources of entangled electrons, where the two electrons in Cooper pair are spin and momentum entangled [2]. Usually, the Andreev reflection (AR) [3] is a local process of converting an electron into a hole occurring at the same interface of a superconductor, producing a Cooper pair in a superconductor. Sometimes, however, the AR can be a nonlocal process [4] and this referred to as the crossed Andreev reflection (CAR), in which the conversion from an electron into a hole occurs at two different interfaces of a superconductor. Therefore, the reverse process of the CAR is a good approach to produce the spatially separated entangled states of electrons by splitting Cooper pairs from the superconducting condensate into two leads [5, 6], and then the entangled states of electrons can be well probed in

experiments. In experiments, a tunable Cooper pair splitter with high efficiency has been realized in low-dimensional semiconductor structures [7]; furthermore, a close-to-unity efficiency has already been achieved [8].

Usually, the CAR competes with other transport processes, such as the normal reflection (NR), local Andreev reflection (LAR), and the elastic cotunneling (EC) in conventional metal–superconductor–metal (MSM) heterostructures. EC is a process that the electron tunnels elastically from one lead to the other through the superconducting energy gap. EC often has the same probability as the CAR in MSM junctions [4, 9], thus the CAR cannot be detected by nonlocal conductance. Recently, several proposals have been raised to make the signatures of CAR clearly observable in conductance. The pure CAR was predicted in an n-type graphene–superconductor–p-type graphene junction for a particular bias voltage [10]. A perfect CAR was suggested in a superconducting graphene spin valve for all bias voltages in superconducting energy gap [11]. Nonlocal Cooper pair splitting has been proposed in a p-type semiconductor–superconductor–n-type semiconductor junction by means of the band gap of a semiconductor [12]. The CAR has also studied in systems based on topological insulators (TIs) [13–21]. The change from pure EC to pure CAR has been studied in a superconducting spin valve based on a 3D TI, which is controlled by the configuration of magnetizations [17]. A resonant CAR was predicted in a junction based on a narrow quantum spin Hall insulator [18]. Furthermore, a Majorana fermion induced resonant CAR has been inspected in a 1D topological superconductor [20].

In this paper, we study the nonlocal transport of a ferromagnet–superconductor–ferromagnet (FSF) junction on the surface of a TI, where the magnetizations in the left and right leads are perpendicular to the surface. So far the electrically controlled nonlocal transport of this system has not been addressed, and it is found to be very interesting. The nonlocal transport process can be pure CAR, which appears for all bias voltages in the superconducting energy gap and is independent of the configuration of the magnetizations of the two leads. The average transmission probability of CAR is very large, therefore high efficiency nonlocal splitting of Cooper pairs can be generated, and turned on and off electrically.

2. Model and formalism

We consider a ballistic 2D FSF junction formed on the surface of a 3D TI as shown in figure 1(a). The bulk s-wave superconductor (S) interacts with the surface electrons of a TI by the proximity effect, and then superconductivity is induced in the topological surface states [22–30]. The ferromagnetism in the surface states is induced by the proximity effect of the ferromagnetic insulator (FI) [31, 32]. The interfaces between ferromagnet and superconductor are parallel to y-direction, and the superconductor segment is located between $x = 0$ and $x = l$ [33]. In the Nambu notation $\Phi = (\Phi_\uparrow, \Phi_\downarrow, \Phi_\downarrow^\dagger, -\Phi_\uparrow^\dagger)^T$, where $\Phi_{\uparrow(\downarrow)}$ is the electron field operator with spin up

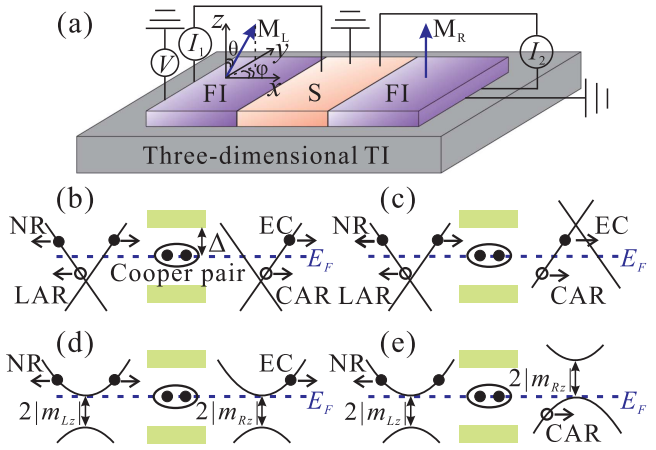

Figure 1. (a) Schematic diagram of a 2D FSF junction on the surface of a 3D TI. (b) and (d) show the energy band of the n-type lead–superconductor–n-type lead junction on the TI surface, (c) and (e) correspond to the energy band of the n-type lead–superconductor–p-type lead junction on the TI surface. The left and right normal-state leads show no gap in (b) and (c), while the left and right ferromagnetic leads have magnetic gaps $2|m_{Lz}|$ and $2|m_{Rz}|$, respectively, in both (d) and (e). The dashed blue lines represent the Fermi energy E_F.

$\uparrow$(down $\downarrow$), the 2D FSF junction can be described by the Bogoliubov–de Gennes equation [34–36],

$$\begin{pmatrix} \hat{h}_+ - \mu(r) & \hat{\Delta} \\ \hat{\Delta}^* & \hat{h}_- + \mu(r) \end{pmatrix} \psi(x, y) = \varepsilon\psi(x, y), \qquad (1)$$

with $\hat{h}_\pm = \pm\upsilon_F \boldsymbol{\sigma} \cdot \mathbf{p} + \boldsymbol{\sigma} \cdot \mathbf{m}(r)$, where the Pauli matrices $\boldsymbol{\sigma} = (\sigma_x, \sigma_y, \sigma_z)$, the in-plane electron momentum $\mathbf{p} = (p_x, p_y, 0)$, the Fermi velocity υ_F, and the chemical potential $\mu(r)$ are measured with respect to the Dirac point. $\psi(x, y)$ is the wave function, and ε is the excitation energy. The magnetization $\mathbf{m}(r)$ is chosen to be a vector pointing along an arbitrary direction in the left region with $\mathbf{m}_L = (m_{Lx}, m_{Ly}, m_{Lz}) = m_L(\sin\theta\cos\varphi, \sin\theta\sin\varphi, \cos\theta)$ and fixed along the z-axis perpendicular to the TI surface in the right region with $\mathbf{m}_R = (0, 0, m_{Rz})$. The chemical potential $\mu(r)$ is μ_S in the middle of the superconducting region, μ_L and μ_R in the left and right ferromagnetic regions, and they three could be tuned independently [37, 38]. $\hat{\Delta} = \Delta e^{i\eta}$ is the superconducting pair potential in the middle region, and Δ and η are the energy gap and phase of the superconductor, respectively.

Solving equation (1), we obtain the wave function in the left ferromagnetic lead as

$$\psi_L = \psi_a e^{ik_x x} + r_e\psi_b e^{-i\left(k_x + \frac{2m_{Lx}}{\hbar\upsilon_F}\right)x} + r_h\psi_c e^{ik'_x x}, \qquad (2)$$

where $\psi_a = (\hbar\upsilon_F k_x + m_{Lx} - i(\hbar\upsilon_F k_y + m_{Ly}), \varepsilon + \mu_L - m_{Lz}, 0, 0)^T$, $\psi_b = (-\hbar\upsilon_F k_x - m_{Lx} - i(\hbar\upsilon_F k_y + m_{Ly}), \varepsilon + \mu_L - m_{Lz}, 0, 0)^T$, and $\psi_c = (0, 0, -\hbar\upsilon_F k'_x + m_{Lx} + i(\hbar\upsilon_F k_y - m_{Ly}), \varepsilon - \mu_L - m_{Lz})^T$. The chemical potential μ_L is taken to lie in the conduction bands and $\mu_L > 0$. Then $k_x = (\sqrt{(\varepsilon + \mu_L)^2 - m_{Lz}^2 - (\hbar\upsilon_F k_y + m_{Ly})^2} - m_{Lx})/\hbar\upsilon_F$, and $k'_x = (\sqrt{(\varepsilon - \mu_L)^2 - m_{Lz}^2 - (\hbar\upsilon_F k_y - m_{Ly})^2} + m_{Lx})/\hbar\upsilon_F$. r_e and r_h are the coefficients of the wave functions for the NR and

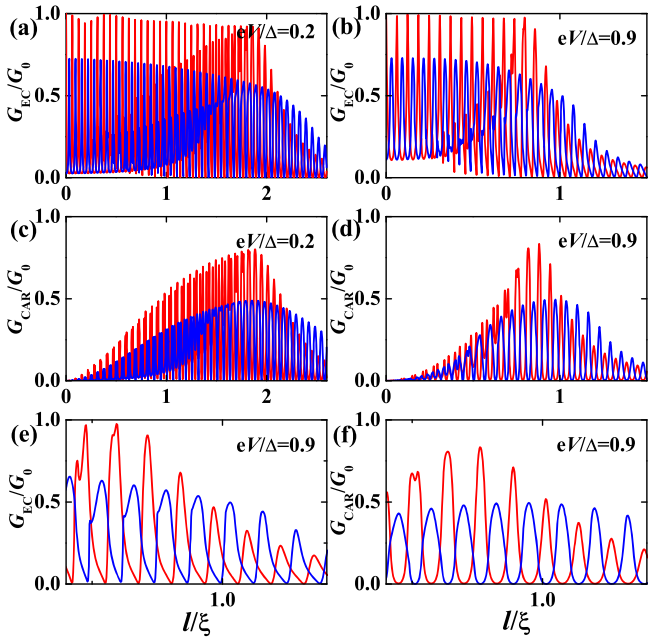

Figure 2. Normalized cross differential conductance as a function of the junction width l. In (a) and (c) $eV/\Delta = 0.2$, in (b) and (d) $eV/\Delta = 0.9$, where $\mu_L = |m_{Lz}| = 10\Delta$ and $\mu_S = 50\Delta$. $\mu_R = |m_{Rz}| = 10\Delta$ in (a) and (b), and $-\mu_R = |m_{Rz}| = 10\Delta$ in (c) and (d). (e) and (f) are parts of (b) and (d), respectively. The red and blue lines correspond to the parallel and antiparallel configurations of the magnetizations in the left and right leads, respectively.

LAR, respectively. We define the incident angle of the electron as $\phi = \arcsin(\hbar v_F k_y + m_{Ly})/(\sqrt{(\varepsilon + \mu_L)^2 - m_{Lz}^2})$. Note that the symbol T in the wave functions indicates transpose.

The chemical potential μ_S is assumed to be very large to accommodate the superconductivity [39]. Then, the wave function in the middle superconducting region is:

$$\psi_S = c\psi_d e^{ik_{x0}x+Kx} + d\psi_e e^{-ik_{x0}x-Kx} + f\psi_f e^{ik_{x0}x-Kx} + g\psi_g e^{-ik_{x0}x+Kx}, \quad (3)$$

where $\psi_d = (e^{i(\eta-\gamma-\alpha)}, e^{i(\eta-\alpha)}, e^{-i\gamma}, 1)^T$, $\psi_e = (-e^{i(\eta+\gamma-\alpha)}, e^{i(\eta-\alpha)}, -e^{i\gamma}, 1)^T$, $\psi_f = (-e^{i(\eta-\gamma+\alpha)}, e^{i(\eta+\alpha)}, e^{-i\gamma}, 1)^T$, and $\psi_g = (-e^{i(\eta+\gamma+\alpha)}, e^{i(\eta+\alpha)}, -e^{i\gamma}, 1)^T$. $k_{x0} = \sqrt{(\mu_S/\hbar v_F)^2 - k_y^2}$, $K = \frac{\mu_S \Delta \sin\alpha}{\hbar^2 v_F^2 k_{x0}}$, $\alpha = \arccos(\varepsilon/\Delta)$ for $\varepsilon < \Delta$, $\gamma = \arcsin(\hbar v_F k_y/\mu_S)$ is the angle of the quasiparticles, and c, d, f, and g are coefficients of the wavefunctions which are coherent superpositions of electron and hole excitations.

The wave function in the right ferromagnetic lead is:

$$\psi_R = t_e\psi_h e^{ik_x'' x} + t_h\psi_i e^{ik_x''' x}, \quad (4)$$

where $\psi_h = (\hbar v_F(k_x'' - ik_y), \varepsilon + \mu_R - m_{Rz}, 0, 0)^T$, and $\psi_i = (0, 0, -\hbar v_F(k_x''' - ik_y), \varepsilon - \mu_R - m_{Rz})^T$. By defining $\Lambda_1 = (\varepsilon + \mu_R)^2 - m_{Rz}^2 - (\hbar v_F k_y)^2$ and $\Lambda_2 = (\varepsilon - \mu_R)^2 - m_{Rz}^2 - (\hbar v_F k_y)^2$, $k_x'' = \sqrt{\Lambda_1}$ for $\mu_R > 0$, and $k_x'' = \mathrm{sgn}(\varepsilon + \mu_R)\sqrt{\Lambda_1}$ for $\mu_R < 0$. $k_x''' = \mathrm{sgn}(\varepsilon - \mu_R)\sqrt{\Lambda_2}$ for $\mu_R > 0$, and $k_x''' = \sqrt{\Lambda_2}$ for $\mu_R < 0$. t_e and t_h are the coefficients of the wave functions for EC and CAR, respectively.

There exists a translational invariance along the y-direction, so the wave vector k_y is conserved in the three regions, and we omit the common part $e^{ik_y y}$ in the above wave functions. These wave functions are matched by the boundary conditions: $\psi_L(0) = \psi_S(0)$ and $\psi_S(l) = \psi_R(l)$, which determine the coefficients r_e, r_h, t_e, and t_h in the wave functions.

A bias voltage is applied in the left ferromagnetic lead, while the superconductor and right ferromagnetic lead are grounded. It is straightforward to get the cross (nonlocal) differential conductance from the nonlocal current I_2 between the superconductor and right ferromagnetic lead at zero temperature as $G = dI_2/dV = G_{EC} - G_{CAR}$ [40], with

$$G_{EC} = \frac{G_0}{2}\int_{-\frac{\pi}{2}}^{\frac{\pi}{2}} T_{EC}(\varepsilon, \phi)\cos\phi \mathrm{d}\phi, \quad (5)$$

$$G_{CAR} = \frac{G_0}{2}\int_{-\frac{\pi}{2}}^{\frac{\pi}{2}} T_{CAR}(\varepsilon, \phi)\cos\phi \mathrm{d}\phi, \quad (6)$$

where $G_0 = \frac{e^2}{h}N(eV)$, $N(eV)$ is the density of states given by $N(\varepsilon) = \frac{w_y\sqrt{(\mu_L+\varepsilon)^2 - m_{Lz}^2}}{\pi\hbar v_F}$. $T_{EC}(\varepsilon, \phi) = \left|\frac{(\varepsilon+\mu_R-m_{RZ})\hbar v_F \mathrm{Re}(k_x'')}{(\varepsilon+\mu_L-m_{Lz})(\hbar v_F k_x + m_{Lx})}\right| t_e(\varepsilon, \phi)t_e^*(\varepsilon, \phi)$, and $T_{CAR}(\varepsilon, \phi) = \left|\frac{(\varepsilon-\mu_R-m_{Rz})\hbar v_F \mathrm{Re}(k_x''')}{(\varepsilon+\mu_L-m_{Lz})(\hbar v_F k_x + m_{Lx})}\right| t_h(\varepsilon, \phi)t_h^*(\varepsilon, \phi)$, which two are the transmission probabilities of EC and CAR, respectively. Here, w_y is the width of the junction along the y-direction, which is much larger than l, and we take ε as eV, where V is the bias voltage.

3. Results and discussion

In the following, we will first study the cross differential conductance of the nonlocal transport when the magnetizations of the left and right ferromagnets are collinear in the z-direction, and then study the influence of the magnetization component along the x- and y-directions on the cross differential conductance.

3.1. Physics of the FSF junction

The surface states of a TI are described by the 2D massless Dirac equation. Therefore, except for a particular excitation energy ε [10], the processes of NR, LAR, EC, and CAR ubiquitously exist for an incident electron in a normal-state lead–superconductor–normal-state lead junction on the TI surface, and such existence is independent of the type of the carriers in the two normal-state leads as shown in figures 1(b) and (c). Due to the spin-momentum locking of the surface states, a magnetic gap will be produced in surface states when the magnetization of the ferromagnet is in the z-direction [41]. Such a magnetic gap in the right lead could make the nonlocal transport to be contributed purely either by EC for $|m_{Rz}| = \mu_R$ as shown in figure 1(d) or by CAR for $|m_{Rz}| = -\mu_R$ as shown in in figure 1(e) when eV takes any value in the superconducting energy gap. If $|m_{Lz}| = \mu_L$, the magnetic gap in the left lead could be used to rule out the LAR as shown in

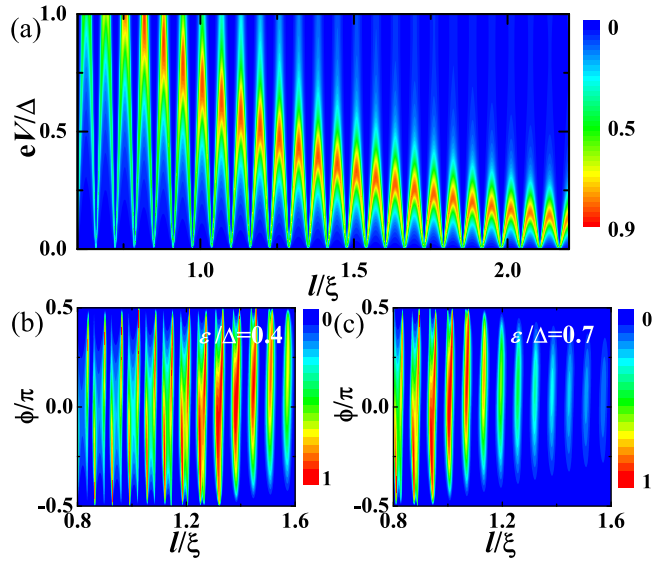

Figure 3. (a) Normalized cross differential conductance G_{CAR}/G_0 as a function of l and V. (b) and (c) Transmission probability T_{CAR} as a function of incident angle ϕ and l. Here $\mu_S = 50\Delta$, $\mu_L = -\mu_R = |m_{Lz}| = |m_{Rz}| = 10\Delta$, and the magnetizations in the left and right leads are in a parallel configuration.

figures 1(d) and (e). Based on the physical illustration in figure 1, we will quantitatively investigate the cross differential conductance G, which is pure G_{EC} or pure G_{CAR}.

3.2. Junction width dependence of G_{EC} and G_{CAR}

In figures 2(a) and (b), we present the conductance G_{EC} as a function of the junction width l which is in the unit of superconducting coherence length $\xi = \hbar v_{\mathrm{F}}/\Delta$. Because of $\mu_R = |m_{Rz}|$, the cross differential conductance is pure G_{EC}. It is found that G_{EC} rapidly oscillates with decaying amplitudes, as l increases. Such an overall decrease of the oscillation magnitude is due to the fact that the conductance G_{EC} results from the tunneling effect in the superconducting energy gap, which is manifested in the part $e^{\pm Kx}$ in the wave function of the superconductor. It is seen that G_{EC} exists in both parallel and antiparallel configurations of the magnetizations, and such a character is different from that of the superconducting graphene spin valve [11] and the superconducting spin valve on the TI surface [17]. The G_{EC} in antiparallel configuration has a shift of about half a period compared with that in the parallel configuration, as shown in figures 2(a) and (b). This anomalous transport results from the fact that the transmission probability of the electron has a shift of about half a period between the parallel and antiparallel configuration, which is similar to that in the ferromagnet–normal–ferromagnet junction on the TI surface [41].

Figures 2(c) and (d) show the dependence of G_{CAR} on the junction width l, where because of $-\mu_R = |m_{Rz}|$, the cross differential conductance is pure G_{CAR}. The G_{CAR} rapidly oscillates with the increase of l, the same as G_{EC}. Such kind of rapid oscillation with l is due to the phase factor $e^{\pm \mathrm{i}k_{x0}x}$ of the wave function in the superconductor, where k_{x0} is proportional to μ_S when μ_S is large enough. The dependence of G_{CAR} on l is basically different from that of G_{EC} as can be seen by comparing figure 2(c) with figure 2(a) or 2(d) with figure 2(b). It can clearly be seen that the oscillation magnitude of G_{CAR} first increases and then decreases with the increase of l, which is rooted in two aspects below. On the one hand, the increase of G_{CAR} with l stems from the fact that the CAR is a process converting an electron into a hole, which needs a sufficiently long superconductor for the formation of coherence of two electrons as a Cooper pair. On the other hand, the following decrease of G_{CAR} with l results from the fact that the CAR occurs nonlocally at two different superconductor interfaces. It is of interest that the conductance G_{CAR} exists in both parallel and antiparallel configurations. On the whole, the envelope of G_{CAR}'s oscillation with l is unimodal, which is different from the multimodal character of that in superconducting graphene spin valves [11]. Such a difference is due to the enhanced CAR and the prohibited EC occurring in the bands having originated from the same Dirac cone for the junction on the TI surface, while they are from two different Dirac cones for the junction on graphene.

In figure 2, we find that the cross differential conductance which is pure G_{EC} or pure G_{CAR} depends on the carrier's type in the right ferromagnetic lead, rather than on the configuration of the magnetizations in two leads. Hence, the switch between pure EC and pure CAR can be controlled electrically in our proposed setup, such as by gate voltage. Thus, the switch between pure EC and pure CAR in our setup is completely different from magnetically controlled switches in superconducting graphene spin valves [11], in which the change from pure G_{EC} to pure G_{CAR} is proposed by reversing the magnetization direction in one of the ferromagnetic leads.

In [17], the change from pure EC to pure CAR is proposed by altering the configuration of the magnetizations from parallel to antiparallel under the assumption that the magnetizations in the two leads are in the x–y plane. The magnetization in the x–y plane cannot open the gap in the surface states of TIs. However, the y-orientations of the magnetizations shift the Fermi surfaces in the two leads. When the y-orientations of the magnetizations in two leads are parallel (antiparallel), the Fermi surface of the incident electrons matches well only with the Fermi surface of the electrons (holes) for EC (CAR), thus the only nonlocal transport process is EC (CAR). In figure 2, the magnetizations in the two leads are in z-orientation, which can open a gap in the surface states. Pure EC happens in both parallel and antiparallel configurations of the magnetizations, so does pure CAR. Whether the nonlocal transport process is pure EC or pure CAR depends on the carrier's type in the right ferromagnetic lead, thus the switch between pure EC and pure CAR is controlled electrically. In other words, the mechanism of the nonlocal transport proposed in our setup is novel and absolutely different from that in [17].

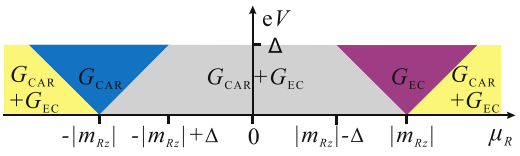

Figure 4. Dependence of the cross differential conductance on V and μ_R for fixed $|m_{Rz}|$, where $|m_{Rz}| \geqslant \Delta$, $|m_{Lz}| = |m_{Rz}|$, and $\mu_L = |\mu_R|$ or $\mu_L = |m_{Lz}|$. Gray indicates zero G_{EC} and G_{CAR}, yellow indicates nonzero G_{EC} and G_{CAR}. And purple and blue indicate nonzero pure G_{EC} and pure G_{CAR}, respectively.

Since the maximum magnitude of the conductance G_{CAR} occurs around the junction width $l \sim \xi$ as shown in figures 2(c) and (d), next we will carefully consider the influence of the bias voltage V on G_{CAR} around $l \sim \xi$. In figure 3(a), the dependence of the conductance G_{CAR} on the junction width l is shown for all bias voltages V in the superconducting energy gap Δ. We find that the width l at which the maximum magnitude of G_{CAR} appears becomes short with the increase of the bias voltage V. This behavior can be clearly understood from the properties of transmission probability T_{CAR}. Figures 3(b) and (c) show the dependence of T_{CAR} on ϕ and l for two different excitation energies ε, respectively. It is found that T_{CAR} mainly oscillates with l and changes slightly with ϕ. And the width l at which the maximum value of T_{CAR} appears becomes short with the increase of the excitation energy ε by comparing figures 3(b) and (c). The nonlocal differential conductance G_{CAR} is proportional to the summation of the transmission probability T_{CAR} over all incident angles.

3.3. Dependence of cross differential conductance on chemical potential

When the magnetizations in the left and right leads are collinear in the z-direction, the cross differential conductance that is pure G_{CAR} for all bias voltages $0 < eV < \Delta$ is satisfied under the assumption of $\mu_L = -\mu_R = |m_{Lz}| = |m_{Rz}| \geqslant 0.5\Delta$. Moreover, the cross differential conductance that is pure G_{CAR} can also be obtained for the bias voltages $x < eV/\Delta < 1$ under the condition $\mu_L + (-)x\Delta = -\mu_R + (-)x\Delta = |m_{Lz}| = |m_{Rz}|$ for $|m_{Rz}| \geqslant \Delta$ and $0 < x < 1$. The condition for pure G_{EC} could be obtained similarly as for G_{CAR}. As shown in figure 4, the cross differential conductance can be abruptly switched from pure G_{EC} (pink) to pure G_{CAR} (blue) by changing μ_R, where μ_R could be tuned by gate voltage. Hence, the magnitudes of μ and m_z in the left and right leads do not have to be equal and much larger than Δ, and the observation and control of CAR are easy to implement in experiments.

Although the width l of the superconductor in the FSF junction is unchangeable in experiments, it is convenient to tune the chemical potential μ_S of the superconductor. Now, we consider the influence of μ_S on the conductance G_{CAR}. Figure 5 shows that G_{CAR} changes periodically with the increase of μ_S. Such a periodicity results due to the fact that, for large μ_S, the factor γ appearing in the spinor part of wave function is nearly zero, and k_{x0} in $e^{ik_{x0}x}$ is proportional to μ_S.

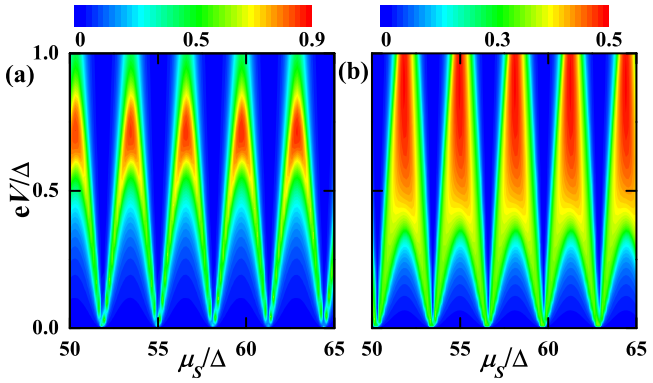

Figure 5. Normalized cross differential conductance G_{CAR}/G_0 as a function of V and μ_S, where $\mu_L = -\mu_R = |m_{Lz}| = |m_{Rz}| = 10\Delta$, and $l = \xi$. (a) and (b) correspond to parallel and antiparallel configuration, respectively.

So, the period will certainly increase with the decrease of the width l of the superconductor. Comparing figure 5(a) with figure 5(b), it is seen that the maximum magnitude of G_{CAR} in the parallel configuration is larger than that in the antiparallel configuration, and G_{CAR} is large in the parallel configuration while it is small in the antiparallel configuration and vice versa.

Note that, in figures 2, 3 and 5, the normalized conductance G_{CAR}/G_0 reflects the average transmission probability of the conversion from an incident electron into a crossed Andreev reflected hole at the given energy, and the conversion probability is found to be very large. Hence, a very high efficiency nonlocal splitting of Cooper pairs could be generated and well tuned in our proposed model.

3.4. Role of spin-triplet pairing correlation

As shown above, the CAR occurs in both the parallel and antiparallel configurations, which is unusual and essentially different from that in a similar junction based on graphene because the operator $\boldsymbol{\sigma}$ in the Dirac Hamiltonian represents real spin and pseudospin for topological surface states and graphene, respectively. Since the Cooper pairs are spin-singlet pairing correlation in superconducting graphene spin valves [11], the spin of the incident electron is antiparallel to the spin of the crossed Andreev reflected hole for the formation of a Cooper pair. But for topological surface states, the proximity effect of the s-wave spin-singlet superconductor always induces both spin-singlet and spin-triplet Cooper pairs [34, 42–44]. In figure 1(b), the spin of the incident electron in the left lead is parallel to $(k_x, k_y, 0)^T$, and the spin of the hole in the right lead is parallel to $(k_x''', -k_y, 0)^T$. So on the one hand, when k_y is small, the spins of the incident electron and the hole of the CAR are approximately parallel, which is supported by the spin-triplet Cooper pairs. On the other hand, when k_y is large, the spins of the incident electron and the crossed Andreev reflected hole are approximately antiparallel, which is supported by the spin-singlet pairing Cooper pairs. In figure 1(c), the spin of the incident electron in the left lead is parallel to $(k_x, k_y, 0)^T$, and the spin for the hole in the right lead is parallel to $(k_x''', k_y, 0)^T$. So in general, the spins of the incident electron and the crossed

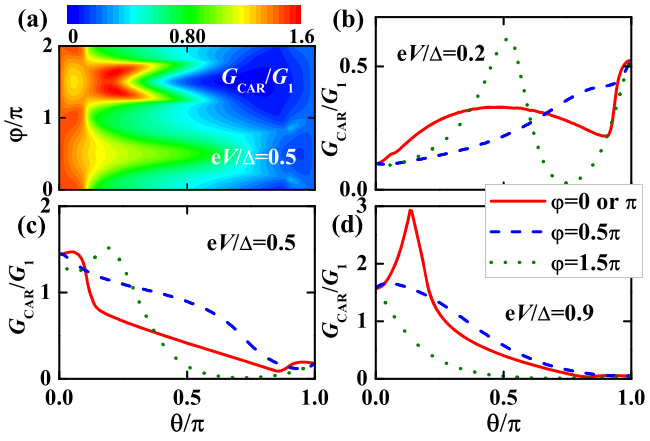

Figure 6. Conductance G_{CAR}/G_1 as a function of the direction angle θ at different azimuth angles φ of the left ferromagnet for different bias voltages V, where $\mu_L = -\mu_R = |m_L| = m_{Rz} = 10\Delta$, $l = \xi$, $\mu_S = 50\Delta$, and $G_1 = e^2 w_y/(h\pi)$.

Andreev reflected hole are approximately parallel, which is supported by the spin-triplet Cooper pairs. In figure 1(e), the magnetizations interact with the spins to affect the direction of the spins of the electron and hole in the two leads, therefore, the spin of the incident electron is parallel to $(k_x, k_y, m_{Lz}/\hbar\upsilon_F)T$, and the spin of the crossed Andreev reflected hole is parallel to $(k_x''', k_y, m_{Rz}/\hbar\upsilon_F)^T$. Therefore, when m_{Lz} and m_{Rz} are large enough as given in the above figures and satisfy $m_{Lz} = m_{Rz}$ ($m_{Lz} = -m_{Rz}$), the spins of the incident electron and the hole of the CAR are approximately parallel (antiparallel), which is supported by the spin-triplet (spin-singlet) Cooper pairs.

3.5. Effect of x- and y-components of magnetization on G_{CAR}

Finally, we consider the effect of the x- and y-components of the magnetization in the left lead on the conductance G_{CAR}, as shown in figure 6, where the magnetization is in the z-direction in the right lead. In figure 6(a), the conductance G_{CAR} depends irregularly on θ and φ of the magnetization in the left ferromagnet. Concretely, we present the effect of the x- or y-component of the magnetization in figures 6(b), (c), and (d), in which the magnetization stays in x-z or y-z plane. We find the x-component of the magnetization has no effect on G_{CAR}, and the change of G_{CAR} with θ for the curves with $\varphi = 0$ or π just displays the effect of m_{Lz} on G_{CAR}. When $\theta = 0.5\pi$ and $\varphi = 0$ or π, the left ferromagnetic surface state is equivalent to a normal topological surface state, and the G_{CAR} has a finite value. Such a character means that the pure CAR can be observed in a normal-state–superconductor–ferromagnet junction on a TI surface, which is different from the junction in [17] where two magnetic leads are needed and must be in an antiparallel configuration. By comparing the curves for $\varphi = 0.5\pi$ or 1.5π with those for $\varphi = 0$, we find the y-component magnetization has a remarkable effect on G_{CAR}, and such an influence depends on both the magnitude and direction of m_{Ly}. Also it can be seen that the change in G_{CAR} with m_{Lz} and m_{Ly} is irregular, and depends obviously on the bias voltage V as shown in figures 6(b), (c), and (d). Hence, pure CAR can be obtained when one of the two ferromagnetic leads become normal topological surface states in our setup.

In our calculations, constant finite singlet pairing Δ is used in equation (1) to explore the nonlocal transport. Interesting results have been shown in a wide range of widths l, which ranges from 0–2.6ξ in figure 2 and from 0.6ξ–2.2ξ in figure 3(a). Certainly, the magnetism has influence on the amplitude and the uniformity of Δ in a superconductor, thus the uniformity of Δ would be difficult to be realized in real life setups. However, our results are not obtained at a fixed width of the superconductor, such as $l = \xi$. If $l = \xi$ is not sufficiently long to maintain the superconductivity, it could be double and even triple that of ξ. Therefore, the uniformity and detailed amplitude of Δ should not change the primary physics in our model. In order to establish a model which will well simulate real life setups, one can adopt a piecewise function to describe Δ in a superconducting region in the theoretical calculations.

The conventional superconducting spin valve has been realized in an experiment in [33]. The realization demonstrates that it is possible to have a finite singlet pairing Δ between two oppositely magnetized leads. Fortunately, the superconductivity and the magnetism of the topological surface states have been realized step by step in experiments [22, 32].

4. Conclusions

In this paper, we have studied the nonlocal quantum transport of the FSF junction on the surface of a TI. It has been found that the switch between pure CAR and pure EC can be controlled electrically, and pure CAR is independent of the configuration of the magnetizations in the left and right leads. Such a pure CAR could occur for all bias voltages in the superconducting energy gap. The average transmission probability of CAR could be very large, hence, a very high efficiency nonlocal splitting of Cooper pairs could be produced. The spin of the crossed Andreev reflected hole can be generally parallel to the spin of the incident electron, which is induced by the spin-triplet pairing correlation.

Moreover, we would like to discuss the realization of our model. The bulk band gap of a TI depends on the materials, which are, for example, about 300 meV in Bi_2Se_3, 100 meV in Bi_2Te_3, and 22 meV in HgTe [45–48]. The magnetic gap of the surface states could be realized by putting the magnetic material on the surface of a TI. The magnetic material could be MnSe or $MnBi_2Se_4$. Depending on the interface match of the TI and magnetic material, the surface gap can be 54 meV for a Bi_2Se_3/MnSe heterostructure and 100 meV for a $MnBi_2Se_4/Bi_2Se_3$ heterostructure [32, 49]. The superconducting energy gap of the surface states could be induced by depositing the superconductor on the surface of a TI. The superconducting energy gap of the surface states is about 1.1 meV for the $Bi_2Se_3/NbSe_2$ and $Bi_2Te_3/NbSe_2$ junctions, and 0.07 meV for the HgTe/Nb junction [22, 50, 51]. The gate electrode and chemical doping have been used to tune the

chemical potential of the surface states of Bi_2Se_3, Bi_2Te_3, or HgTe in experiments [37, 38, 51–53]. The superconducting coherence length ξ of the surface states is about 200–2000 nm for $\upsilon_F = 5 \times 10^5\ m\ s^{-1}$ [45, 50], then the width of the superconducting region in our model can be about 200–2000 nm. Thus at present, the parameters and calculated values in our work can be accessible in a real life system. We suggest that Bi_2Se_3 and Bi_2Te_3 could be good candidates for the 3D TI materials in our setup.

Acknowledgments

We acknowledge the insightful discussions with Zhen-Gang Zhu, Zheng-Chuan Wang, Qing-Rong Zheng, and Gang Su. This work is supported in part by the National Natural Science Foundation of China (Grant Nos. 11704366, 10934008, and 10974253), the China Postdoctoral Science Foundation (Grant No. 2016M590569), and the Natural Science Foundation of Shandong Province (Grant No. ZR2017QA009).

ORCID iDs

Kunhua Zhang https://orcid.org/0000-0002-8200-6777

References

[1] Zeilinger A 1999 *Rev. Mod. Phys.* **71** S288
Galindo A and Martín-Delgado M A 2002 *Rev. Mod. Phys.* **74** 347
[2] Burkard G, Loss D and Sukhorukov E V 2000 *Phys. Rev.* B **61** 16303(R)
Lesovik G B, Martin T and Blanter G 2001 *Eur. Phys. J.* B **24** 287
Samuelsson P, Sukhorukov E V and Büttiker M 2003 *Phys. Rev. Lett.* **91** 157002
[3] Andreev A F 1964 *Sov. Phys. JETP* **19** 1228
[4] Byers J M and Flatte M E 1995 *Phys. Rev. Lett.* **74** 306
[5] Recher P, Sukhorukov E V and Loss D 2001 *Phys. Rev.* B **63** 165314
[6] Herrmann L G, Portier F, Roche P, Yeyati A L, Kontos T and Strunk C 2010 *Phys. Rev. Lett.* **104** 026801
[7] Hofstetter L, Csonka S, Nygård J and Schönenberger C 2009 *Nature* **461** 960
[8] Schindele J, Baumgartner A and Schönenberger C 2012 *Phys. Rev. Lett.* **109** 157002
[9] Falci G, Feinberg D and Hekking F W J 2001 *Eurohys. Lett.* **54** 255
[10] Cayssol J 2008 *Phys. Rev. Lett.* **100** 147001
[11] Linder J, Zareyan M and Sudbø A 2009 *Phys. Rev.* B **80** 014513
[12] Veldhorst M and Brinkman A 2010 *Phys. Rev. Lett.* **105** 107002
[13] Hasan M Z and Kane C L 2010 *Rev. Mod. Phys.* **82** 3045
Qi X L and Zhang S C 2011 *Rev. Mod. Phys.* **83** 1057
Moore J E 2010 *Nature* **466** 15
[14] Nilsson J, Akhmerov A R and Beenakker C W J 2008 *Phys. Rev. Lett.* **101** 120403
[15] Law K T, Lee P A and Ng T K 2009 *Phys. Rev. Lett.* **103** 237001
[16] Sato K, Loss D and Tserkovnyak Y 2010 *Phys. Rev. Lett.* **105** 226401
[17] Niu Z P 2010 *J. Appl. Phys.* **108** 103904
[18] Chen W, Shen R, Sheng L, Wang B G and Xing D Y 2011 *Phys. Rev.* B **84** 115420
[19] Vali R and Khouzestani H F 2014 *Eur. Phys. J.* B **87** 25
[20] He J J, Wu J, Choy T P, Liu X J, Tanaka Y and Law K T 2014 *Nat. Commun.* **5** 3232
[21] Li K and Zhang Y Y 2016 *Phys. Rev.* B **94** 165441
[22] Wang M X *et al* 2012 *Science* **336** 52
[23] Qu F *et al* 2012 *Sci. Rep.* **2** 339
[24] Zareapour P *et al* 2012 *Nat. Commun.* **3** 1056
[25] Maier L, Oostinga J B, Knott D, Brüne C, Virtanen P, Tkachov G, Hankiewicz E M, Gould C, Buhmann H and Molenkamp L W 2012 *Phys. Rev. Lett.* **109** 186806
[26] Zhang K H, Zhu Z G, Wang Z C, Zheng Q R and Su G 2014 *Phys. Lett.* A **378** 3131
[27] Xu S Y *et al* 2014 *Nat. Phys.* **10** 943
[28] Sun H H *et al* 2016 *Phys. Rev. Lett.* **116** 257003
[29] Islam S K F, Dutta P and Saha A 2017 *Phys. Rev.* B **96** 155429
[30] Breunig D, Burset P and Trauzettel B 2018 *Phys. Rev. Lett.* **120** 037701
[31] Wang Y *et al* 2017 *Nat. Commun.* **8** 1364
[32] Hirahara T *et al* 2017 *Nano Lett.* **17** 3493
[33] Gu Y, Halász G B, Robinson J W A and Blamire M G 2015 *Phys. Rev. Lett.* **115** 067201
[34] Fu L and Kane C L 2008 *Phys. Rev. Lett.* **100** 096407
Fu L and Kane C L 2009 *Phys. Rev. Lett.* **102** 216403
[35] Akhmerov A R, Nilsson J and Beenakker C W J 2009 *Phys. Rev. Lett.* **102** 216404
[36] Tanaka Y, Yokoyama T and Nagaosa N 2009 *Phys. Rev. Lett.* **103** 107002
Linder J, Tanaka Y, Yokoyama T, Sudbø A and Nagaosa N 2010 *Phys. Rev.* B **81** 184525
[37] Steinberg H, Laloë J B, Fatemi V, Moodera J S and Herrero P J 2011 *Phys. Rev.* B **84** 233101
[38] Wang Y *et al* 2012 *Nano. Lett.* **12** 1170
[39] Beenakker C W J 2006 *Phys. Rev. Lett.* **97** 067007
[40] Blonder G E, Tinkham M and Klapwijk T M 1982 *Phys. Rev.* B **25** 4515
[41] Zhang K H, Wang Z C, Zheng Q R and Su G 2012 *Phys. Rev.* B **86** 174416
[42] Black-Schaffer A M and Balatsky A V 2013 *Phys. Rev.* B **87** 220506(R)
[43] Zhang K, Zeng J, Ren Y and Qiao Z 2017 *Phys. Rev.* B **96** 085117
[44] Beiranvand R, Hamzehpour H and Alidoust M 2017 *Phys. Rev.* B **96** 161403(R)
[45] Zhang H, Liu C X, Qi X L, Dai X, Fang Z and Zhang S C 2009 *Nat. Phys.* **5** 438
[46] Xia Y *et al* 2009 *Nat. Phys.* **5** 398
[47] Chen Y L *et al* 2010 *Science* **329** 659
[48] Brüne C, Liu C X, Novik E G, Hankiewicz E M, Buhmann H, Chen Y L, Qi X L, Shen Z X, Zhang S C and Molenkamp L W 2011 *Phys. Rev. Lett.* **106** 126803
[49] Luo W and Qi X L 2013 *Phys. Rev.* B **87** 085431
[50] Xu J P *et al* 2014 *Phys. Rev. Lett.* **112** 217001
[51] Wiedenmann J, Liebhaber E, Kübert J, Bocquillon E, Burset P, Ames C, Buhmann H, Klapwijk T M and Molenkamp L W 2017 *Phys. Rev.* B **96** 165302
[52] Tu N H, Tanabe Y, Satake Y, Huynh K K and Tanigaki K 2016 *Nat. Commun.* **7** 13763
[53] Bathon T, Achilli S, Sessi P, Golyashov V A, Kokh K A, Tereshchenko O E and Bode M 2016 *Adv. Mater.* **28** 2183